Articles

Interaction and Properties of Highly Exfoliated Soy Protein/ Montmorillonite Nanocomposites

Pu Chen and Lina Zhang*

Department of Chemistry, Wuhan University, Wuhan 430072, China

Received December 4, 2005; Revised Manuscript Received March 5, 2006

The soy protein isolate (SPI)/ Na^+−montmorillonite (MMT) plastics were successfully prepared, and their structures and properties were characterized with X-ray diffraction, transmission electron microscopy, differential scanning calorimetry, thermogravimetric analysis, and tensile testing. The interactions between the soy protein macromolecules and MMT in aqueous media were analyzed with ζ-potential measurements, Fourier transform infrared spectroscopy, and electrostatic surface potential calculations. The results revealed that the heterogeneous distribution of the surface positive charges provided the positive-charge-rich domains for the soy globulins bearing net negative charges to anchor into the negatively charged MMT galleries. There were electrostatic attraction and hydrogen bonding interactions on the interfaces of the soy protein and MMT, which led to the good dispersion of the phyllosilicate layers in the protein matrix. The highly exfoliated MMT layers with a dimension of 1−2 nm in thickness were randomly dispersed in the protein matrix containing MMT lower than 12 wt %, whereas the intercalated structure was predominant when the MMT content was higher than 12 wt %. Consequently, the fine dispersion of the MMT layers and the strong interactions between SPI and MMT created the significant improvement of the mechanical strength and thermo-stability of the SPI/MMT plastics. In addition, a schematic illustration was proposed to describe the electrostatic interaction between SPI and MMT as well as the correlation between the interaction and structure in protein/clay systems.

Introduction

In recent years, montmorillonite (MMT) has attracted great industrial and academic interests because of its high aspect ratio of silicate nanolayers, its high surface area, and the wide application in the field of polymer materials.[1,2] Structurally, the polymer/MMT nanocomposites can be divided into *intercalated* and *exfoliated* morphologies.[3] As is well-known, the dispersion scale of the phyllosilicate in the polymer matrix is strongly responsible for the efficiency of the clay as a reinforcing filler.[4] Accordingly, the process and mechanism of the highly exfoliated polymer/clay nanocomposites have been a focus in the fields of fundamental and application research.[5−11] There are three dominant ways to achieve exfoliated nanocomposites, that is, solution intercalation, melt intercalation, and in situ intercalative polymerization.[12−14] For the development of fundamental research and the commercial request, highly exfoliated polymer/MMT nanocomposites obtained in a direct and low-cost way become more and more attractive.[15,16]

In the past decade, protein-based "green" materials have become a research focus because of their high performance, low cost, and eco-friendly characteristics.[17−20] In all of the protein sources, soy protein has been regarded as a readily renewable biopolymer and potential source for biodegradable plastics and adhesives.[21−25] Its commercial raw material is soy protein isolate (SPI) with more than 90% protein and 18 diverse amino acids.[26] It is noted that plastics made from SPI alone possesses good biodegradable performance but poor flexibility. Therefore, plasticizers are usually used to overcome the brittleness of the SPI plastics, which unavoidably leads to the significant decrease of its tensile strength.[27] To obtain the flexible materials having high strength, some suitable reinforcing fillers have been involved in the SPI/plasticizer systems.[21,28−30] Some high-performance natural polymer/clay materials with a intercalated or highly exfoliated structure have been achieved by several research groups.[31−36] However, as far as we know, the preparation and characterization of highly exfoliated soy protein/clay nanocomposite materials have not been reported till now. The high affinity of clays to proteins and amino acids bearing neutral, positive, and even negative charges were observed in soils, which hints at the possibility to prepare SPI/MMT nanocomposite materials.[36−38] In light of molecular biology, soy protein is mainly composed of glycinin and β-conglycinin.[39,40] Five major subunits of glycinin have been identified and classified into two groups according to their amino acid sequences (group I: A1aB1b, A2B1a and A1bB2; group II: A3B4 and A5A4B3). On the other hand, β-conglycinin has three kinds of subunits, namely α, α′, and β.[39] According to the recent achievement of the well-defined amino acid sequences and detailed architectures of soy protein, it is possible to investigate the mechanism of the interaction between soy protein and MMT at a molecular level.

A basic understanding of the molecular interaction and structure in protein nanocomposites is essential for the fundamental research and development of protein-based materials. In the present study, the highly exfoliated and intercalated SPI/

* Corresponding author. Tel.: +86-27-87219274; Fax: +86-27-6875-4067. E-mail: lnzhang@public.wh.hb.cn.

10.1021/bm050924k CCC: $33.50
Published on Web 05/03/2006

MMT nanocomposite plastics were prepared, and the correlation between the structure and properties was investigated. Moreover, the interaction of the SPI and MMT in aqueous media was analyzed with ζ-potential measurements, Fourier transform infrared spectroscopy (FT-IR), and electrostatic potential calculations. The object of this paper was to clarify the interactions between the soy protein and MMT layers as well as the effects of the microstructures on the properties of the nanocomposites.

Experimental Part

Materials. Commercial SPI was purchased from DuPont−Yunmeng Protein Technology Co. Ltd. (Yunmeng, China). The weight-average molecular weight (M_w) of SPI was determined by a multi-angle laser light scattering instrument (MALLS, DAWN DSP, Wyatt Technology Co., USA) equipped with a He−Ne laser ($\lambda = 632.8$ nm) to be 2.05×10^5. The origin moisture content, protein content, and amino acid compositions of SPI have been investigated and detailed in our previous paper.[26] Na^+-montmorillonite (MMT, NANNOLIN DK0) was supplied by Fenghong Clay Chemical Corporation in China. The cation exchange capacity of this Na^+-MMT was 110 meq/100 g with a particle dimension of 25 × 1000 nm in dry state. Glycerol purchased from the Shanghai Chemical Co. (Shanghai, China) was of analytical grade.

Preparation of MMT/SPI Nanocomposites and Plastic Sheets. A total of 10 g of SPI was dissolved in 160 mL of distilled water at ambient temperature with stirring to obtain an emulsion. At the same time, a desired amount of MMT was dispersed in 40 mL of distilled water and stirred for 30 min. The MMT suspension was then added into the SPI emulsion with severe stirring at 60 °C for 2 h. The resultant light-yellow viscous liquid was centrifuged with a speed of 9000 rpm at 25 °C for 15 min. The precipitate after centrifugation was suspended in 100 mL of acetone and then filtered. Subsequently, the resulting sample was vacuum-dried for 24 h to obtain a yellow nanocomposite powder. By controlling the MMT content to be 0, 4, 8, 12, 16, 20, and 24 wt %, the nanocomposite powders obtained were coded as MP-0, MP-4, MP-8, MP-12, MP-16, MP-20, and MP-24, respectively.

The MP-series powders with an addition of 30 wt % glycerol as plasticizer were beaten up in a high-speed mixer (HR1704, PHILIPS Ltd., Zhuhai, China) for 15 min, and then were mixed further with a single-screw extruder (PolyDrive with Rheomex R252, ThermoHaake, Germany) with a diameter of 19.1 mm and a length/diameter ratio of 25:1. The screw rotation speed was 30 rpm, and the temperature profile along the extruder barrel was 80, 100, and 120 °C (from feed zone to exit). Subsequently, the mixture of the SPI/MMT nanocomposties and glycerol were compression-molded at 140 °C and 20 MPa. The resultant plastic sheets were coded as MS-0, MS-4, MS-8, MS-12, MS-16, MS-20, and MS-24, respectively. The nanocomposite powders and plastic sheets were conditioned in a desiccator with P_2O_5 as the desiccant for one week at room temperature before characterization.

Characterization. The pH values of the SPI/MMT nanocomposite suspension were obtained by using a pH analyzer (Lida, pHS-25, China). ζ-potential analysis was carried out on a Zetasizer 3000HSA apparatus (Malven, England). The suspensions with varying MMT contents for the pH-value and ζ-potential analyses were prepared through a process as the preparation of the SPI/MMT nanocomposite. In this case, the concentration of the nanocomposites in aqueous suspension was fixed to be 0.1%. Fourier transform infrared spectroscopy (FT-IR) was recorded on a Nicolet 5700 spectrometer (Nicolet, U.S.A.) in the range of 4000−400 cm^{-1} using a KBr pellet method. The electrostatic surface potential distribution was calculated and visualized by a Swiss PdbViewer 3.7 (SP5) program using the Coulomb law.[41] The pH value of the aqueous media in the calculation was fixed at 7.4. The contouring values of the potential were set as −1.8 kT/e for the negative potential and 1.8 kT/e for the positive potential, and the negative and positive potentials were colored in blue and red, respectively. In this case, only charged residues (Arg, Lsy, Glu, and Asp) were taken into account for their contribution to the surface potential, and the charges were located at the corresponding (non-H) atom positions. The original files of the amino acid sequences for the α_c', β, and A1aB1b homotrimers were downloaded from the RCSB Protein Data Bank. The face with the interchain disulfide bond (IE face) and that with the intrachain disulfide bond (IA face) were shown as two typical faces of the three-dimensional structures for homotrimers.

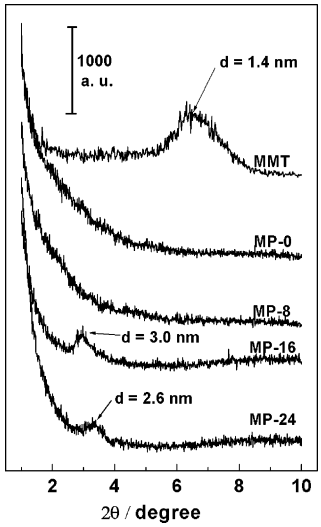

Figure 1. XRD patterns of MMT and nanocomposites with various MMT contents.

X-ray diffraction (XRD) was performed on a D8 Advance diffractometer (Bruker, U.S.A.) equipped with a Cu Kα radiation source ($\lambda = 0.154$ nm). The diffraction data were collected from $2\theta = 1 \sim 10°$ in a fixed time mode with a step interval of 0.02°. The structure and morphology of the nanocomposite powders and plastics were visualized by a transmittance electron microscope (TEM) [JEM-2010 FEF (UHR), JEOL, Japan] at an accelerating voltage of 200 kV. The SPI/MMT powder samples with a concentration of 0.1 mg mL^{-1} were suspended in acetone and then dispersed on a Formbar-backed carbon-coated copper grid. Ultrathin sections of the SPI/MMT plastics were prepared using a Leica Ultracut UCT with EMFCS cryo-attachment at −120 °C. The cross-sections with the thickness of ∼60 nm were obtained by using a diamond knife. The ultrathin films of the samples were directly placed on the copper grids.

The glass transition behaviors of the nanocomposite sheets were analyzed on a differential scanning calorimetry (DSC) analyzer (DSC-204, Netzsch Co., Germany) equipped with a liquid-nitrogen-cooling system and was calibrated with an indium standard ($T_f = 156.6$ °C). O-ring-sealed stainless steel capsules with high-pressure resistance (40 bar) were used to eliminate the interfering of the heat of evaporating. The sample in capsule was quenched to −100 °C and then heated to 180 °C under nitrogen atmosphere with a heating rate of 20 °C min^{-1}. Thermogravimetric analysis (TGA) of the SPI/MMT nanocomposite sheets was investigated on a STA 499C instrument (NETZSCH Co., Germany) under a nitrogen atmosphere from 30 to 800 °C at a heating rate of 10 °C min^{-1}. The tensile strength (σ_b), elongation at break (ϵ_b), and Young's modulus (E) of the sheets were measured on a universal testing machine (CMT6503, Shenzhen SANS Test Machine Co. Ltd., Shenzhen, China) with a tensile rate of 5 mm min^{-1} according to ISO527−3:1995(E). Five parallel measurements were carried out for each sample.

Results and Discussion

Structure of SPI/MMT Nanocomposites. The structure and apparent interlayer spacing (d spacing) of the SPI/MMT nanocomposites prepared via solution intercalation have been detected by X-ray diffraction. Figure 1 shows the XRD patterns for the MMT and the nanocomposites. The basal spacing of

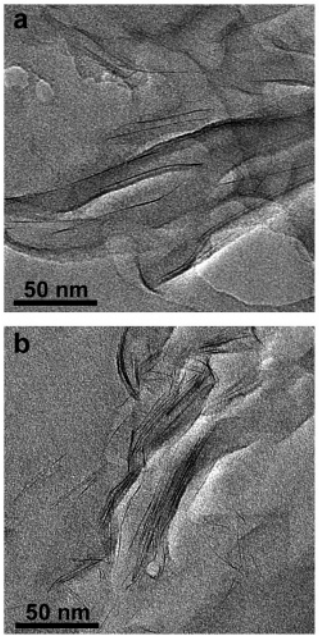

Figure 2. TEM images of MP-8 (a) and MP-24 (b).

pristine MMT has been calculated to be 1.4 nm from a diffraction peak at $2\theta = 6.4°$ using Bragg function. The MMT-free MP-0 shows no diffraction peak in the 2θ range from 1 to 10°, showing that the soy protein has no ordered structure in this dimension range. The diffraction peak of the MMT tactoids is absent in the X-ray diffraction spectrum when the MMT content reaches 8 wt % for MP-8. This suggests that the MMT layers are highly disordered in the nanocomposite powders. In the cases of MP-16 and MP-24 powders, the diffraction peaks in the XRD patterns reveal an intercalated structure with the *d*-spacing values of about 3.0 and 2.6 nm. This indicates that the layered MMT is delaminated in the aqueous medium by the soy protein macromolecules as the MMT content is relatively low, whereas the intercalated structure of MMT in soy protein matrixes is dominant when the MMT content is higher than 16 wt %. This phenomenon accords with the conclusion raised by Ray and Okamoto about the dependence of the nanocomposite structure (exfoliated or intercalated) on the MMT content.[12]

TEM studies are necessary to verify the extent of delamination and exfoliation achieved.[42] Figure 2 presents the TEM images of MP-8 (a) and MP-24 (b). In Figure 2a, the MMT layers are well dispersed in the soy protein matrix. Although the MMT layers still retain their orientation to some degree, the MMT tactoids are highly delaminated into some thin lamellas by soy protein with a dimension of about 1∼2 nm in thickness. When the MMT content is up to 24 wt %, the layered structure of the MMT is generally intercalated in the soy protein matrix. The *d*-spacing values increase from 1.4 nm for the pristine MMT to a value ranging from 2 to 3 nm, which is in good agreement with the results from the XRD experiments. On the basis of the evidence from XRD and TEM, the SPI/MMT nanocomposites with a highly delaminated or intercalated structure have been successfully prepared via a solution intercalation process in the neutral aqueous media without any special aid. Moreover, the results obviously suggest a high affinity between soy protein and MMT. It should be assigned to some kind of interaction, such as an electrostatic interaction and/or hydrogen bonding.

Interaction between Soy Protein and MMT. The dependence of the pH values of the SPI suspensions on the MMT contents is shown in Figure 3. When the MMT addition increases from 0 to 24 wt %, the pH values of the suspensions

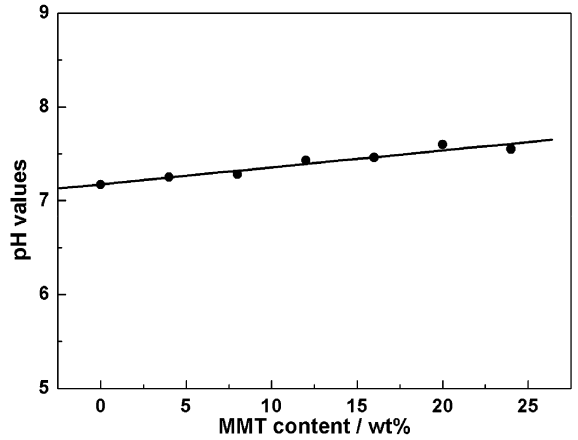

Figure 3. Dependence of pH value of SPI/MMT suspensions on MMT content.

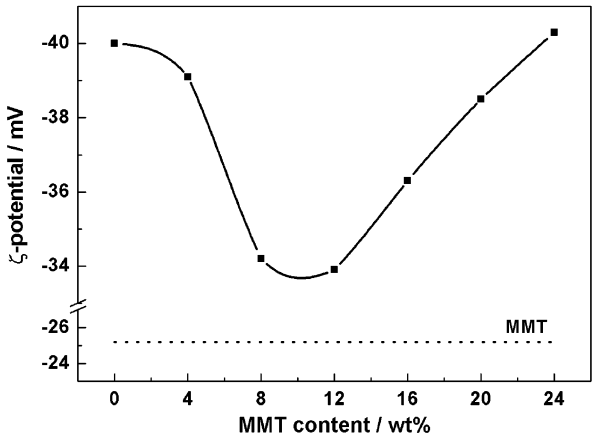

Figure 4. Dependence of ζ potential of SPI/MMT particles on MMT contents.

slowly increase from 7.17 to 7.55. This suggests that the addition of MMT hardly changes the electrostatic surface potential of the soy protein molecules. Figure 4 shows the ζ potential of the SPI/MMT nanocomposites with various MMT contents. The ζ-potential values of the pure SPI and the MMT particles are −40.0 and −25.2 mV, respectively. In the MMT content range of 0∼12 wt %, the larger ζ-potential values of the SPI/MMT particles than those of the pure MMT particles indicate the effective covering of the SPI onto the exfoliated MMT layers as shown in Figure 2a. Usually, the larger ζ-potential values provide higher stability of the colloidal particles in aqueous media. The results from the ζ-potential measurement prove that the electrostatic interaction between soy protein and MMT stabilizes the MMT layers in aqueous media. The decrease of the ζ-potential values suggests that the amount of protein molecules on the SPI/MMT micelles drops as the MMT content increases from 0 to 12 wt %.[43] However, the apparent potential values abnormally increase from −34.2 to −39.6 mV when the MMT content is higher than 12 wt %. In the preparation process of the SPI/MMT suspension with the MMT content higher than 12 wt %, the conglomeration of the SPI/MMT nanocomposites has been actually observed in the suspension. So the large ζ potential in the high MMT content cases could be ascribed to the contribution of the free protein particles in the aqueous media. In the range of the MMT content from 0 to 24 wt %, the nonlinear change of the ζ-potential values evidently reflects the existence of the electrostatic interaction between the SPI biopolymers and layered MMT.[44]

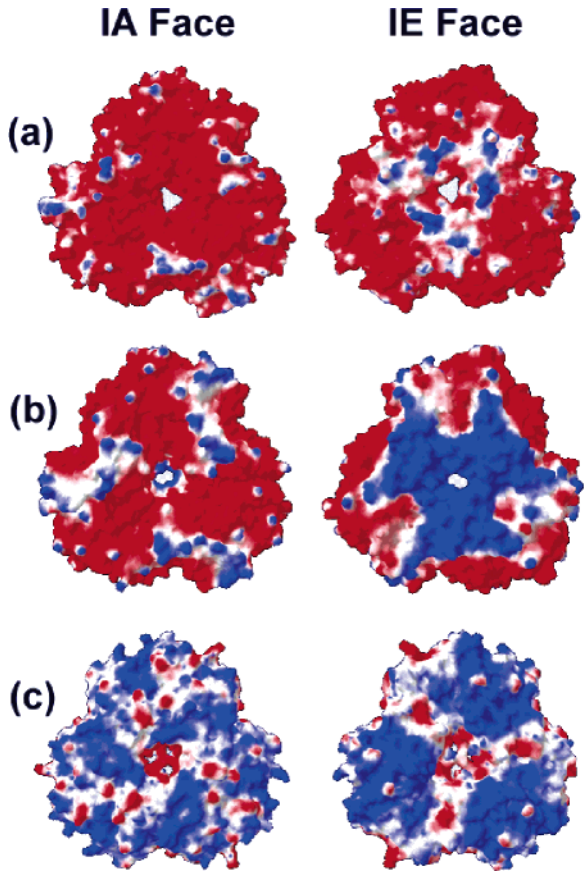

Figure 5. Distribution of electrostatic surface potential of three typical homotrimers of soy protein at pH = 7.4, (a) β homotrimer of β-conglycinin, (b) α' homotrimer of β-conglycinin, and (c) A1aB1b homotrimer of glycinin. Left column is IA faces, and right column is IE faces. The negative potential (<−1.8 kT/e) is colored in red and positive potential (>1.8 kT/e) is colored in blue.

In view of the interesting results from the XRD, TEM, and ζ-potential analyses, the soy proteins with net negative charges exhibit very high affinity to the negatively charged MMT layers. Some other researches dealing with the absorption of protein molecules into clays have shown analogous results; that is, some slightly negatively charged or neutral proteins can enter the galleries of mineral clays and broaden the interlamellar spaces.[37,45] For both glycinin and β-conglycinin of soy protein, each subunit of them consists of an acidic polypeptide and a basic polypeptide. So, one of the possible explanations for these "unreasonable" results could lie in the electrostatic potential distribution on the soy protein surfaces. Figure 5 illustrates the electrostatic surface potential distribution of three typical soy protein homotrimers aligned by A1aB1b, α_c', and β subunits. Because of the selected contouring values of the potential (−1.8 kT/e for the negative potential and 1.8 kT/e for the positive potential), only charged residues (Arg, Lsy, Glu, and Asp) are taken into account for their contribution to the surface potential.[41] It is obvious that the negative electrostatic potential predominates on the IE and IA faces of β-conglycinin β homotrimer and the IA face of the α_c' homotrimer, whereas the positive charges are dotted on these surfaces. However, the IE face of the β-conglycinin α_c' homotrimer as well as the IE and IA faces of the glycinin A1aB1b homotrimers are highly positively charged, and furthermore, the positive charges are mainly confined in some specific domains. In nature, the heterogeneous distribution of the electrostatic surface potential is of great benefit to the construction of the quaternary structures from the protein subunits.[40] In this case, although the net charge of the soy protein

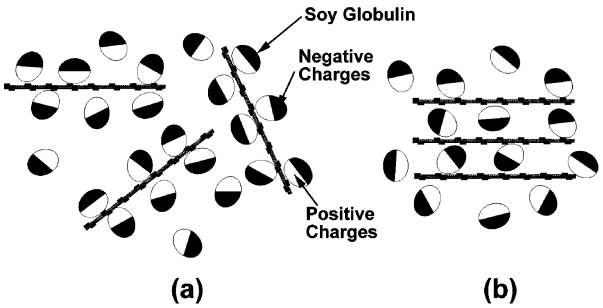

Figure 6. Schematic illustration of the electrostatic interaction between soy globulins and MMT, (a) highly exfoliated state and (b) intercalated state. Positively charged domains are colored in white, and negatively charged domains are in black.

particles is negative, the heterogeneous dispersion of the positive and negative charges causes the existence of the positive-charge-rich domains on the homotrimer's surfaces, which provide the active positively charged sites for the replacement of Na^+ and for the anchoring of the soy protein molecules into the negatively charged MMT galleries. Figure 6 presents a schematic illustration of the electrostatic interaction between soy protein and MMT with highly exfoliated and intercalated structures. Figure 6a shows that the highly exfoliated MMT layers are well covered by soy proteins. The positive-charge-rich domains of the globulins are attracted by the negatively charged surfaces of the silicate layers. For the intercalated structure, the soy protein molecules bearing positive-charge-rich and negative-charge-rich domains expand the negatively charged MMT galleries. Therefore, the contact area between MMT and soy protein is highly diminished as shown in Figure 6b.

As is well-known, the C═O-containing molecules and amide are able to form hydrogen bonding with the polar groups on the MMT layered surfaces.[46] Structurally, the surface of the MMT galleries contains Si−O−Si and −OH groups which could act as hydrogen bonding sites for the guest molecules.[46,47] The effects of hydrogen-bonding should be taken into account for the intercalation of protein molecules into the negatively charged MMT. The FT-IR spectra in at 1800∼1600 and 1300∼950 cm^{-1} for the MMT, MP-0, MP-8, MP-16 and MP-24 nanocomposite powders are shown in Figure 7. The strong bands at 1656 and 1541 cm^{-1} are assigned to the amide I (C═O stretching) and amide II (N−H bending and C−N stretching modes) absorbance.[48,49] Compared with the amide bands of the MP-0, the bands of the amide I and amide II for the MP-8 with a highly exfoliated structure become multiple. This result indicates the existence of the hydrogen bonding between the soy protein peptide bonds and the polar groups, such as −OH and Si−O−Si on the surface of MMT layers. However, these changes are more and more unobvious as the MMT content reaches 16 and 24 wt %, which is caused by the decreasing amount of the contact protein molecules per MMT layer while the structure of the nanocomposites shifts from the highly delaminated to the intercalated one. The absorbant bands of the Si−O stretching are presented in Figure 7b. Because of the low symmetry of the dioctahedral MMT layer, the Si−O absorbance of Na^+-MMT is split into four individual peaks at 1120 (peak I), 1087 (peak II), 1040 (peak III) and 1014 (peak IV) cm^{-1}. Peaks I, III, and IV are assigned to the in-plane Si−O stretching bands.[50] It is noted that peak II at 1087 cm^{-1} ascribed to the out-of-plane vibration is related to the orientation of the MMT layers. Especially, the disordering of the clay lamellas should cause the increase of the intensity of this band, which has been well proven by the polarized attenuated total reflectance (ATR)-

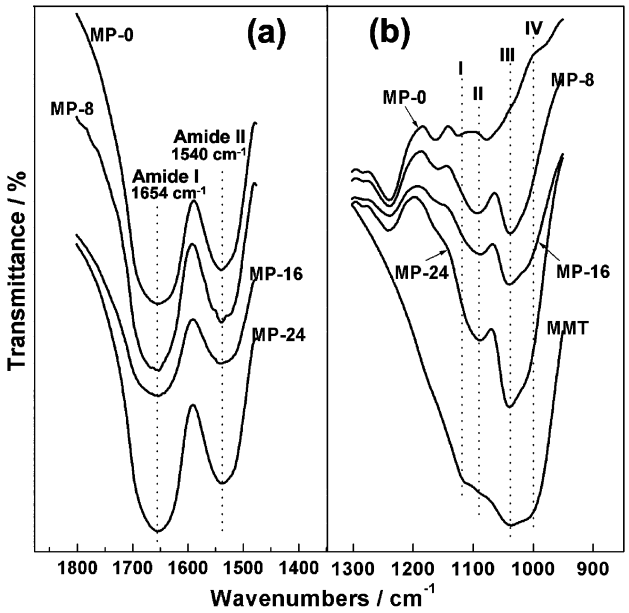

Figure 7. FT-IR spectra at 1800∼1600 cm^{-1} (a) and 1300∼950 cm^{-1} (b) for MMT, MP-0, MP-8, MP-16, and MP-24.

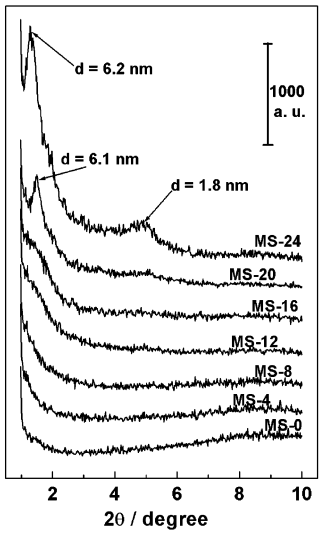

Figure 8. XRD patterns of MS-series sheets with various MMT contents.

FTIR experiments.[50,51] In this case, the pristine Na^+-MMT presents a unobvious absorbance, whereas the out-of-plane Si−O vibration absorbance of the SPI/MMT nanocomposites becomes sharp and separated. This distinct change means the orientation structure of MMT has been strongly perturbed by the soy protein molecules. In view of the obvious change of the protein amide II absorbance and the Si−O stretching peak II, it is believed that the hydrogen bonding exists in the SPI/MMT nanocomposites and the hydrogen bonding sites are the oxygen atoms on the silicate layer surface and the hydrogen atoms in the peptide bonds.[52]

Till now, we conclude that the heterogeneous distribution of the surface positive charges provides the possibility for negatively charged soy protein to intercalate and exfoliate layered MMT, and at least two types of interactions, the surface electrostatic interaction and hydrogen bonding, are involved in the high affinity between soy protein and Na^+-montmorillonite.

Correlation between Structure and Properties. With 30 wt % glycerol as plasticizer, the SPI/MMT plastic sheets have been obtained through a compression-molding process at 140 °C and 20 MPa. The XRD patterns of the nanocompostie plastics (MS-0 to MS-24) with the MMT contents from 0 to 24 wt % are presented in Figure 8. The absence of the diffraction peaks for MS-0, MS-4, MS-8, and MS-12 with the increasing MMT content from 0 to 12 wt % indicates that the high-degree disordering structure of SPI/MMT nanocomposite is maintained in the compression-molding process. The delaminated-intercalated structure transformation is evidenced by the more and more obvious diffraction peaks of the MS-16, MS-20, and MS-24 with relatively high MMT contents. In addition, the diffraction peak of MS-24 shifts to a lower angle ($2\theta \approx 1.4°$), indicating a higher interlayer spacing of 6.2 nm. This phenomenon implies that a melt intercalation process is involved when the nanocomposites are extruded and compression-molded.[53] The microstructure of SPI/MMT plastics has been visualized by using TEM, and the images are shown in Figure 9. When the structures of the MP-8 powder (Figure 2a) and the MS-8 plastic sheet (Figure 9a) are compared, the delaminated silicate lamellas in the MS-8 plastics are further randomized during the extruding and compression-molding process. The dimensions of the silicate layers are diminished to about 30 nm in length and 1 nm in thickness. It indicates the layered MMT is highly exfoliated by the soy protein molecules in the MS-8 plastics. For the MS-16 plastic sheet (Figure 9b), most of the layered MMT tactoids are intercalated with a *d*-spacing of about 6 nm. Simultaneously, some conglomerations of MMT occur in the soy protein matrix. When the MMT content is up to 24 wt %, the degree of the conglomeration becomes serious in the MS-24, leading to the obvious phase separation between soy protein and MMT.

Figure 10 presents the DSC thermograms of the MS-series SPI/MMT plastics. The MS-0 sheet exhibits two glass transitions (T_{g1} and T_{g2}) at −33.2 and 91.5 °C. According to our previous works,[26,54] T_{g1} of the glycerol-plasticized soy protein plastics is assigned to the glass transition temperature of the glycerol-rich domains and T_{g2} to the protein-rich domains. The T_{g2} related

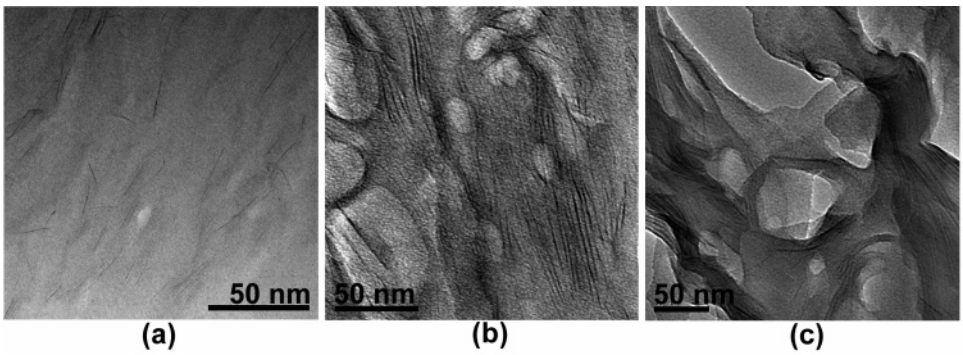

Figure 9. TEM images of SPI/MMT plastics, (a) MS-8, (b) MS-16, and (c) MS-24.

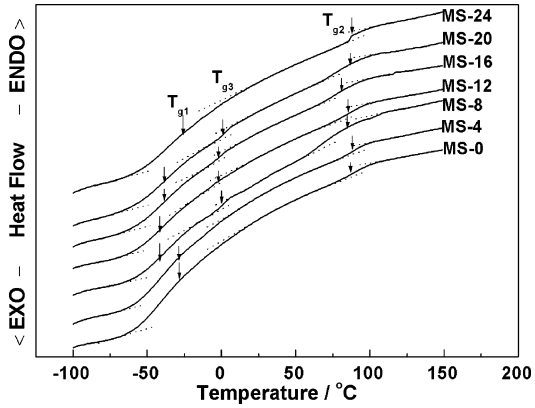

Figure 10. DSC thermograms of MS-series SPI/MMT plastics.

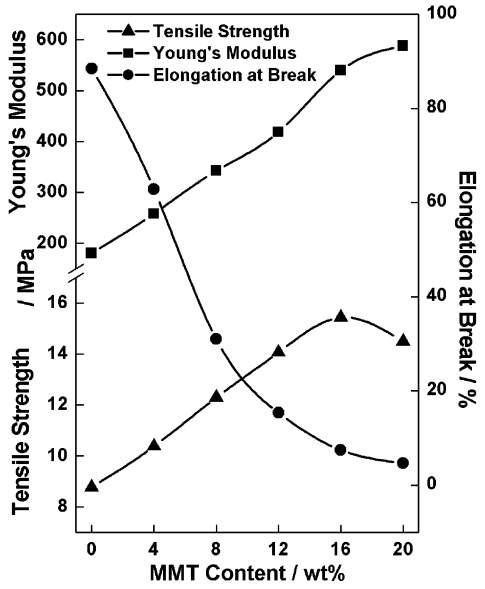

Figure 11. Effects of MMT contents on tensile strength, Young's modulus and elongation at break for SPI/MMT plastics.

to the protein chains and segments with a low compatibility to glycerol and water is almost invariable for all of the SPI/MMT sheets. However, in the cases of the MS-8, MS-12, MS-16, and MS-20 sheets, the T_{g1} is split into two individual ones. The new glass transition (T_{g3}) at −0.6 to ∼+1.6 °C appears as a "shoulder" for T_{g1}. The occurrence of T_{g3} indicates that the delaminated and intercalated MMT layers mainly exist in the glycerol-rich domains of the SPI/MMT nanocomposite sheets. The fine dispersion of MMT layers effectively restricts the segmental motion of the soy protein molecules on the interface of the clay layers because of their high aspect ratio and reactive surface,[55] which is similar to the biopolymer/nanoscale whisker system.[56−58] When the MMT content reaches 24 wt %, the T_{g3} disappeared in the MS-24 samples. This agrees with the TEM and XRD results and points out that the serious phase separation diminishes the interaction between soy protein molecules and MMT layers.

Figure 11 shows the tensile testing results of the SPI/MMT plastic sheets. The MS-24 was omitted from the tensile testing because it is too brittle to be cut into bar-shape testing specimens. The values of the Young's modulus (E) increase from 180.2 to 587.6 MPa with an increase of the MMT content from 0 to 20 wt %. The tensile strength (σ_b) of the sheets improves from 8.77 MPa for the MS-0 to 15.43 MPa for the MS-16. However, when the MMT content reaches 20 wt %, the σ_b value decreases to be 14.48 MPa. These results further

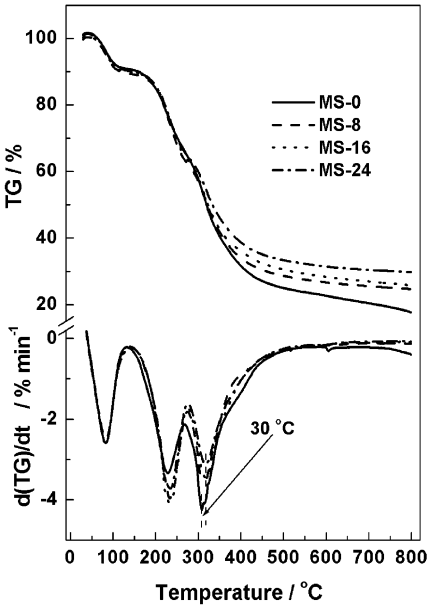

Figure 12. TG traces and dTG curves of MS-0, MS-8, MS-16, and MS-24.

support that the phase separation phenomenon occurs in the SPI/MMT system with a MMT higher content higher than 16 wt %.[3] In the whole MMT content range, the elongation at break (ϵ_b) keeps decreasing with the increase of the MMT addition. All of these results confirm that the strong electrostatic and hydrogen bonding interactions between the soy protein and the highly dispersed MMT layers are significant to restrict the segmental motion of the soy protein, and this restriction leads to the improvement of the modulus and tensile strength of the soy protein plastics.

The thermal stability was investigated by using TGA, and the weight loss traces and their differential curves recorded in the 30−800 °C range are shown in Figure 12. The weight loss between 0 and 120 °C is attributed to the water absorbed in SPI/MMT plastics.[26,54] Such a weight loss is about 9% for all of the samples. The weight loss in the temperature range of 120−250 °C is mainly related to the evaporation of glycerol.[26,54] Clearly, the temperature of the maximum weight-loss rate determined by the peak of the dTG curves for the nanocomposite plastics is 30 °C higher than that of the MMT-free MS-0. The residue weight during the whole thermo-degradation period of soy protein is higher for nanocomposite plastics than that of MS-0. These facts evidence the improvement of thermo-stability in the protein-degradation range of 250−800 °C for the SPI/MMT plastics. All of the results from XRD, TEM, tensile testing, DSC, and TGA deduce a conclusion that the highly exfoliated or intercalated SPI/MMT plastics with improved mechanical strength and thermo-stability have been successfully prepared from the solution-intercalated SPI/MMT nanocomposites via the extrusion mixing and compression molding methods. As a result of the well dispersion of MMT layers in SPI matrixes, the electrostatic and hydrogen bonding interactions between the soy protein and MMT layers play an important role in the improvement of the mechanical and thermal properties of the SPI/MMT plastics.

Conclusion

The biodegradable SPI/MMT plastics with highly exfoliated and intercalated structures have been successfully prepared from

the SPI/MMT nanocomposite obtained via a solution intercalation process in neutral aqueous medium. The structures of both the SPI/MMT nanocomposites and the plastics were strongly depended on the MMT content. When the MMT content was lower than 12 wt %, the MMT were highly exfoliated into single layers with a thickness of approximately 1∼2 nm, whereas the intercalation structure predominated in the SPI/MMT nanocomposites when the MMT content was higher than 12 wt %. The electrostatic surface potential calculation revealed that the heterogeneous distribution of the surface positive charges provided the possibility for negatively charged soy protein to intercalate and exfoliate MMT. In view of the results from the ζ-potential measurement and FT-IR, two kinds of interactions existed in this protein/MMT system, that is, the surface electrostatic interaction between the positive-charge-rich domains of soy protein and the negatively charged MMT layers as well as the hydrogen bonding between the −NH and Si−O groups. Such two interactions were beneficial to the intercalation and delamination of the MMT layers in the soy protein matrixes. Accordingly, the mechanical strength and thermo-stability of the SPI/MMT plastics were significantly improved as a result of the fine dispersion of the MMT layers and the strong restriction effects on the interfaces.

Acknowledgment. This work was supported by a grant from the National Natural Science Foundation of China (20474048), and the Key Laboratory of Cellulose Chemistry, Guangzhou Institute of Chemistry, Chinese Academy of Sciences. The authors are thankful to the Center for Electron Microscopy of Wuhan University.

References and Notes

(1) Lepoittevin, B.; Pantoustier, N.; Devalckenaere, M.; Alexandre, M.; Kubies, D.; Calberg, C.; Jérôme, R.; Dubois, P. *Macromolecules* **2002**, *35*, 8385−8390.
(2) Morlat-Therias, S.; Mailhot, B.; Gonzalez, G.; Gardette, J. *Chem. Mater.* **2005**, *17*, 1072−1078.
(3) Giannelis, E. P. *Adv. Mater.* **1996**, *8*, 29−35.
(4) Viville, P.; Lazzaroni, R.; Pollet, E.; Alexandre, M.; Dubois, P. *J. Am. Chem. Soc.* **2004**, *126*, 9007−9012.
(5) Plummer, C. J. G.; Garamszegi, L.; Leterrier, Y.; Rodlert, M.; Månson, J. E. *Chem. Mater.* **2002**, *14*, 486-488.
(6) Choi, Y. S.; Choi, M. H.; Wang, K. H.; Kim, S. O.; Kim, Y. K.; Chung, I. J. *Macromolecules* **2001**, *34*, 8978−8985.
(7) Viville, P.; Lazzaroni, R.; Pollet, E.; Alexandre, M.; Dubois, P.; Borcia, G.; Pireaux, J. *Langmuir* **2003**, *19*, 9425−9433.
(8) Park, J. H.; Jana, S. C. *Macromolecules* **2003**, *36*, 2758−2768.
(9) Mariott, W. R.; Chen, E. Y.-X. *J. Am. Chem. Soc.* **2003**, *125*, 15726−15727.
(10) Robello, D. R.; Yamaguchi, N.; Blanton, T.; Barnes, C. *J. Am. Chem. Soc.* **2004**, *126*, 8118−8119.
(11) Zhang, Z.; Zhang, L.; Li, Y.; Xu, H. *Polymer* **2005**, *46*, 129−136.
(12) Ray, S. S.; Okamoto, M. *Prog. Polym. Sci.* **2003**, *28*, 1539−1641.
(13) Burnside, S. D.; Giannelis, E. P. *Chem. Mater.* **1995**, *7*, 1597−1600.
(14) Strawhecher, K. E.; Manias, E. *Chem. Mater.* **2000**, *12*, 2943−2949.
(15) Chou, C.; Lin, J. *Macromolecules* **2005**, *38*, 230−233.
(16) Wang, K.; Wang, L.; Wu, J.; Chen, L.; He, C. *Langmuir* **2005**, *21*, 3613−3618.
(17) Wu, Q.; Sakabe, H.; Isobe, S. *Ind. Eng. Chem. Res.* **2003**, *42*, 6765−6773.
(18) Wu, Q.; Yoshino, T.; Sakabe, H.; Zhang, H.; Isobe, S. *Polymer* **2003**, *44*, 3909−3919.
(19) Wu, Q.; Sakabe, H.; Isobe, S. *Polymer* **2003**, *44*, 3901−3908.
(20) Rhim, J.; Lee, J. *Food Sci Biotechnol.* **2004**, *13*, 728−732.
(21) Lu, Y.; Weng, L.; Zhang, L. *Biomacromolecules* **2004**, *5*, 1046−1051.
(22) Liu, Y.; Li, K. *Macromol. Rapid Commun.* **2002**, *23*, 739−742.
(23) Liu, Y.; Li, K. *Macromol. Rapid Commun.* **2004**, *25*, 1835−1838.
(24) X. Mo, X. S. Sun, Y. Wang, *J. Appl. Polym. Sci.* **2001**, *73*, 2595−2602.
(25) Lin,Y.; Hsieh, F.; Huff, H. E. *J. Appl. Polym. Sci.* **1997**, *65*, 695−703.
(26) Chen, P.; Zhang, L. *Macromol. Biosci.* **2005**, *5*, 237−245.
(27) Zhang, J.; Mungara, P.; Jane, J. *Polymer* **2001**, *42*, 2569−2578.
(28) Chen, P.; Zhang, L.; Peng, S.; Liao, B. *J. Appl. Polym. Sci.* **2006** in press.
(29) Liu, W.; Mohanty, A. K.; Askeland, P.; Drzal, L. T.; Misra, M. *Polymer* **2004**, *45*, 7589−7596.
(30) Liu, W.; Mohanty, A. K.; Drzal, L. T.; Misra, M. *Ind. Eng. Chem. Res.* **2005,** *44*, 7105−7112.
(31) Darder, M.; Colilla, M.; Ruiz-Hitzky, E. *Chem. Mater.* **2003**, *15*, 3774−3780.
(32) Huang, M.; Yu, J.; Ma, X. *Polymer* **2005**, *46*, 3157−3162.
(33) Park, H.; Liang, X.; Mohanty, A. K.; Misra, M.; Drzal, L. T. *Macromolecules* **2004**, *37*, 9076−9082.
(34) Park, H.; Misra, M.; Drzal, L. T.; Mohanty, A. K. *Biomacromolecules* **2004**, *5*, 2281−2288.
(35) Joly, S.; Garnaud, G.; Ollitrault, R.; Bokobza, L. *Chem. Mater.* **2002**, *14*, 4202−4208.
(36) Rhim, J.; Lee, J.; Kwak, H. *Food Sci. Biotechnol.* **2005**, *14*, 112−116.
(37) De Cristofaro, A.; Violante, A. *Appl. Clay Sci.* **2001**, *19*, 59−67.
(38) Newman, S. P.; Di Cristina, T.; Coveney, P. V. *Langmuir* **2002**, *18*, 2933−2939.
(39) Adachi, M.; Takenaka, Y.; Gidamis, A. B.; Mikami, B.; Utsumi, S. *J. Mol. Biol.* **2001**, *305*, 291−305.
(40) Adachi, M.; Kanamori, J.; Masuda, T.; Yagasaki, K.; Kitamura, K.; Mikami, B.; Utsumi, S. *Proc. Natl. Acad. Sci. U.S.A.* **2003**, *100*, 7395−7400.
(41) Guex, N.; Peitsch, M. C. *Electrophoresis* **1997**, *18*, 2714−2723.
(42) Yoonessi, M.; Toghiani, H.; Kingery, W. L.; Pittman, C. U., Jr. *Macromolecules* **2004**, *37*, 2511−2518.
(43) Hudson, S.; Magner, E.; Cooney, J.; Hodnett, B. K. *J. Phys. Chem. B* **2005**, *109*, 19496−19606.
(44) Ruso, J. M.; Doe, N.; Somasundaran, P. *Langmuir* **2004**, *20*, 8988−8991.
(45) Fusi, P.; Ristori, G. G.; Calamai, L.; Stotzky, G. *Soil Biol. Biochem.* **1989**, *21*, 911−920.
(46) Sohn, J. R.; Kim, J. T. *Langmuir* **2000**, *16*, 5430−5434.
(47) Consultchi, A.; Cordova, I.; Valenzuela, M. A.; Acosta, D. R.; Bosch, P.; Lara, V. H. *Energy Fuels* **2005**, *19*, 1417−1424.
(48) Nahar, S.; Tajmir-Riahi, H. A. *J. Colloid. Interface Sci.* **1996**, *178*, 648−656.
(49) MacDonald, G. M.; Barry, B. A. *Biochemistry* **1992**, *31*, 9848−9856.
(50) Johnston, C. T.; Premachandra, G. S. *Langmuir* **2001**, *17*, 3712−3718.
(51) Ras, R. H. A.; Johnston, C. T.; Franses, E. I.; Ramaekers, R.; Maes, G.; Foubert, P.; De Schryver, F. C.; Schoonheytdt, R. A. *Langmuir* **2003**, *19*, 4295−4302.
(52) Ray, S. S.; Okamoto, K.; Okamoto, M. *Macromolecules* **2003**, *36*, 2355−2367.
(53) Ray, S. S.; Yamada, K.; Okamoto, M.; Ogami, A.; Ueda, K. *Chem. Mater.* **2003**, *15*, 1456−1465.
(54) Chen, P.; Zhang, L.; Cao, F. *Macromol. Biosci.* **2005**, *5*, 872−880.
(55) Lu, H.; Nutt, S. *Macromolecules* **2003**, *36*, 4010−4016.
(56) Anglès, M. N.; Dufresne, A. *Macromolecules* **2000**, *33*, 8344−8353.
(57) Anglès, M. N.; Dufresne, A. *Macromolecules* **2001**, *34*, 2921−2931.
(58) Mathew, A. P.; Dufresne, A. *Biomacromolecules* **2002**, *3*, 609−617.

BM050924K